JACS
JOURNAL OF THE AMERICAN CHEMICAL SOCIETY
Article
pubs.acs.org/JACS

Ex^{2}Box: Interdependent Modes of Binding in a Two-Nanometer-Long Synthetic Receptor

Michal Juríček,[†,⊥] Jonathan C. Barnes,[†,⊥] Edward J. Dale,[†] Wei-Guang Liu,[§] Nathan L. Strutt,[†] Carson J. Bruns,[†] Nicolaas A. Vermeulen,[†] Kala C. Ghooray,[†] Amy A. Sarjeant,[†] Charlotte L. Stern,[†] Youssry Y. Botros,[‡,∥] William A. Goddard, III,*[,§] and J. Fraser Stoddart*[,†]

[†]Department of Chemistry, Northwestern University, 2145 Sheridan Road, Evanston, Illinois 60208, United States

[‡]Intel Laboratories, Building RNB-6-61, 2200 Mission College Boulevard, Santa Clara, California 95054, United States

[∥]National Center for Nano Technology Research, King Abdulaziz City for Science and Technology (KACST), P.O. Box 6086, Riyadh 11442, Kingdom of Saudi Arabia

[§]Materials and Process Simulation Center, California Institute of Technology, 1200 East California Boulevard, Pasadena, California 91125, United States

Supporting Information

ABSTRACT: Incorporation of two biphenylene-bridged 4,4′-bipyridinium extended viologen units into a *para*-phenylene-based cyclophane results in a synthetic receptor that is ∼2 nm long and adopts a box-like geometry. This cyclophane, **Ex^{2}Box^{4+}**, possesses the ability to form binary and ternary complexes with a myriad of guest molecules ranging from long π-electron-rich polycyclic aromatic hydrocarbons, such as tetracene, tetraphene, and chrysene, to π-electron-poor 2,6-dinitrotoluene, 1,2,4-trichlorobenzene, and both the 9,10- and 1,4-anthraquinone molecules. Moreover, **Ex^{2}Box^{4+}** is capable of forming one-to-one complexes with polyether macrocycles that consist of two π-electron-rich dioxynaphthalene units, namely, 1,5-dinaphtho[38]-crown-10. This type of broad molecular recognition is possible because the electronic constitution of **Ex^{2}Box^{4+}** is such that the pyridinium rings located at the "ends" of the cyclophane are electron-poor and prefer to enter into donor−acceptor interactions with π-electron-rich guests, while the "middle" of the cyclophane, consisting of the biphenylene spacer, is more electron-rich and can interact with π-electron-poor guests. In some cases, these different modes of binding can act in concert to generate one-to-one complexes which possess high stability constants in organic media. The binding affinity of **Ex^{2}Box^{4+}** was investigated in the solid state by way of single-crystal X-ray diffraction and in solution by using UV−vis and NMR spectroscopy for 12 inclusion complexes consisting of the tetracationic cyclophane and the corresponding guests of different sizes, shapes, and electronic compositions. Additionally, density functional theory was carried out to elucidate the relative energetic differences between the different modes of binding of **Ex^{2}Box^{4+}** with anthracene, 9,10-anthraquinone, and 1,4-anthraquinone in order to understand the degree with which each mode of binding contributes to the overall encapsulation of each guest.

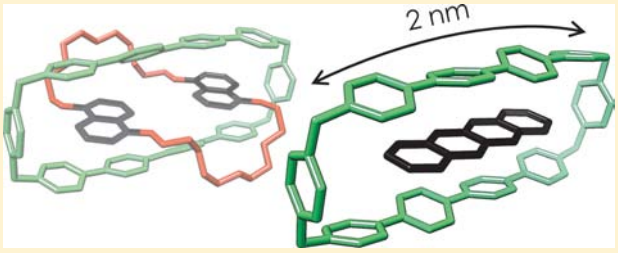

INTRODUCTION

Pedersen's discovery[1] of crown ethers[2] and the subsequent investigation of their ability to bind alkali and alkaline earth metal cations opened the way for synthetic chemists to design molecules that function as selective molecular receptors. His landmark paper was followed by seminal contributions from Cram[3] and Lehn[4] who introduced more complex receptors with the objective of expanding the notion of molecular recognition beyond just the molecule. Their contributions to host−guest[5] and supramolecular[6] chemistry, respectively, laid the foundation upon which macrocyclic receptors have assumed a litany of functions in chemistry.

Some of the more commonly studied synthetic macrocycles, apart from the crown ethers, are the cyclodextrins,[7] cucurbiturils,[8] calixarenes,[9] pillararenes,[10] porphyrins,[11] and cyclophanes,[12] such as cyclobis(paraquat-*p*-phenylene)[13] (**CBPQT^{4+}**). Each of these receptors possesses specific noncovalent modes of binding toward substrates either in the form of (1) ion−dipole interactions, (2) hydrogen bonding, (3) charge-transfer interactions, (4) chelation, and/or (5) contributing hydrophobic effects. Typically speaking, however, most of these macrocycles are capable of binding only guests of similar shape, size, and electronic constitution, that is, either electron-rich or -poor. In order to craft a single macrocycle capable of binding simultaneously a myriad of guests with different shapes and sizes, while also possessing multiple pockets that function using different modes of recognition, a large macrocycle consisting of a diverse electronic architecture—much like that of an enzyme—is required. Here, we

Received: May 25, 2013
Published: July 18, 2013

   dx.doi.org/10.1021/ja4052763 | J. Am. Chem. Soc. 2013, 135, 12736−12746

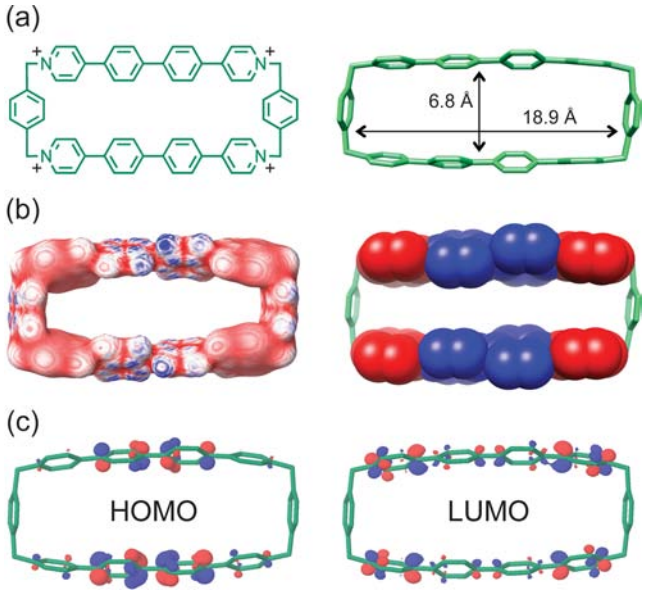

Figure 1. (a) Structural formula of Ex^2Box^{4+} (left) and stick representation of the solid-state structure (right) for $Ex^2Box{\cdot}4PF_6$. (b) Electrostatic potential map (left) and its schematic representation (right) for Ex^2Box^{4+}. Color code: red = relatively lower electron density; and blue = relatively higher electron density. (c) HOMO (left) and LUMO (right) electron density distributions for Ex^2Box^{4+} obtained from DFT calculations.

report the design, synthesis, and versatile binding properties of a large, globally rigid cyclophane, Ex^2Box^{4+} (Figure 1), comprised of two biphenylene-bridged bipyridinium units—also referred[14] to as extended viologens—that is capable of binding π-electron-rich and -poor guests, either as two molecules simultaneously or in the form of long oligoacenes such as tetracene, tetraphene, and chrysene.

EXPERIMENTAL SECTION

The full experimental details are provided in the Supporting Information. Below, the most important information is summarized briefly.

^{1}H NMR Titrations. ^{1}H NMR (298 K, 600 MHz) titrations were performed by adding small volumes of a concentrated guest solution/suspension in either CD_3CN or $CDCl_3$ (depending on solubility) to a solution of $Ex^2Box{\cdot}4PF_6$ in CD_3CN. Tetramethylsilane was used as a reference. Significant upfield shifts of the ^{1}H resonances for β, γ, and δ protons were observed and used to determine the association constants (K_a). The K_a values (M^{-1}) were calculated using Dynafit, a program that employs nonlinear least-squares regression on ligand–receptor binding data.

Ex^2BIPY. A mixture of pyridin-4-ylboronic acid pinacol ester (10.0 g, 48.8 mmol), 4,4′-dibromo-1,1′-biphenyl (6.09 g, 19.5 mmol), $Pd(PPh_3)_4$ (1.13 g, 0.970 mmol), Cs_2CO_3 (22.6 g, 117 mmol), and a 1:1 mixture of dry PhMe/DMF (500 mL) was heated to 130 °C under Ar for 72 h before the hot reaction mixture was rendered acidic (pH 2–3) by adding dropwise concentrated HCl, which caused the crude product to precipitate from solution. Then, the reaction mixture was cooled to room temperature, filtered, and washed with CH_2Cl_2. The solid was dispersed in H_2O at 80 °C, and NaOH solution (10 M) was added dropwise until the pH was ~8–9, resulting in precipitation of the desired product. The solid was filtered and washed with H_2O, dissolved in a 1:1 mixture of hot $CHCl_3$/PhMe and filtered through Celite. The filtrate was concentrated *in vacuo*, yielding pure Ex^2BIPY (4.2 g, 71%) as a white solid. HRMS-ESI for Ex^2BIPY; calcd for $C_{22}H_{16}N_2$: m/z = 309.1386 $[M + H]^+$; found: 309.1383 $[M + H]^+$. ^{1}H NMR (500 MHz, $CDCl_3$, ppm): δ_H 8.70 (AA′ of AA′XX′, J = 6.1, 1.6 Hz, 4H), 7.83–7.78 (AA′BB′, 8H), 7.57 (XX′ of AA′XX′, J = 6.2, 1.6 Hz, 4H). ^{13}C NMR (125 MHz, $CDCl_3$, ppm): δ_C 150.5, 147.8, 141.1, 137.6, 127.9, 127.7, 121.6.

$DB{\cdot}2PF_6$. α,α'-Dibromo-*p*-xylene (5.14 g, 19.5 mmol) was added to a 1:1 mixture of CH_2Cl_2/MeCN (240 mL) in a round-bottomed three-necked flask, and the resulting mixture was heated at 50 °C while stirring until all of the solid material dissolved. Next, the temperature of the oil bath was raised to 90 °C, and a suspension of Ex^2BIPY (600 mg, 1.95 mmol) in MeCN (120 mL) was added in four aliquots slowly over the course of 4 h. After heating under reflux for 24 h, the reaction mixture was cooled to room temperature, and the yellow precipitate was collected by filtration and washed with CH_2Cl_2. The yellow solid was dissolved in cold (≤RT) MeOH (~1 L) followed by the addition of NH_4PF_6 (~400 mg) and cold (≤RT) H_2O (~1 L), resulting in the precipitation of pure $DB{\cdot}2PF_6$ (1.35 g, 72%) that was collected by filtration as a yellowish solid. HRMS-ESI for $DB{\cdot}2PF_6$; calcd for $C_{38}H_{31}Br_2F_{12}N_2P_2$: m/z = 821.0552 $[M - PF_6]^+$; found: 821.0551 $[M - PF_6]^+$. ^{1}H NMR (500 MHz, CD_3CN, ppm): δ_H 8.76 (AA′ of AA′XX′, J = 6.3 Hz, 4H), 8.33 (XX′ of AA′XX′, J = 6.3 Hz, 4H), 8.07 (AA′ of AA′BB′, J = 8.2 Hz, 4H), 8.01 (BB′ of AA′BB′, J = 8.1 Hz, 4H), 7.55 (AA′ of AA′BB′, J = 7.9 Hz, 4H), 7.46 (BB′ of AA′BB′, J = 7.8 Hz, 4H), 5.70 (s, 4H), 4.61 (s, 4H). ^{13}C NMR (125 MHz, CD_3CN, ppm): δ_C 156.9, 145.3, 143.8, 141.1, 134.5, 134.3, 131.1, 130.3, 129.9, 129.3, 126.2, 64.1, 33.5.

$Ex^2Box{\cdot}4PF_6$. A solution of $DB{\cdot}2PF_6$ (600 mg, 0.621 mmol), Ex^2BIPY (192 mg, 0.621 mmol), and the template pyrene (754 mg, 3.73 mmol) in dry MeCN (450 mL) was stirred at RT for 17 d. The reaction was quenched by adding concentrated HCl (2–3 mL), causing the crude product to precipitate from solution. The yellowish precipitate was collected by filtration and dissolved in hot MeOH. The crude $Ex^2Box{\cdot}4PF_6$ was precipitated from solution by adding NH_4PF_6 (~0.5 g) and an excess of H_2O before being subjected to column chromatography using silica gel and CH_2Cl_2/MeCN (1:1) and 0.25–0.5% NH_4PF_6 in MeCN (w/v) as the eluents. Recrystallization in MeCN on slow vapor diffusion of iPr_2O yielded pure $Ex^2Box{\cdot}4PF_6$ (87–104 mg, 10–12%) as a pale-yellow solid. HRMS-ESI of $Ex^2Box{\cdot}4PF_6$; calcd for $C_{60}H_{48}F_{24}N_4P_4$: m/z = 1259.2799 $[M - PF_6]^+$, 557.1576 $[M - 2PF_6]^{2+}$; found: 1259.2792 $[M - PF_6]^+$, 557.1590 $[M - 2PF_6]^{2+}$. ^{1}H NMR (500 MHz, CD_3CN, ppm): δ_H 8.74 (AA′ of AA′XX′, J = 7.0 Hz, 8H), 8.18 (XX′ of AA′XX′, J = 6.9 Hz, 8H), 7.89 (AA′ of AA′BB′, J = 8.6 Hz, 8H), 7.84 (BB′ of AA′BB′, J = 8.6 Hz, 8H), 7.63 (s, 8H), 5.67 (s, 8H). ^{13}C NMR (125 MHz, CD_3CN, ppm): δ_C 156.4, 144.8, 143.4, 137.0, 133.9, 131.0, 129.6, 129.1, 126.0, 64.5.

Crystal Parameters for $Ex^2Box{\cdot}4PF_6$. $[C_{60}H_{48}N_4{\cdot}(PF_6)_4]{\cdot}(MeCN)_2$. Colorless block (0.18 × 0.70 × 0.04 mm). Monoclinic, $P2_1/c$, a = 20.278(8), b = 12.043(5), c = 14.511(7) Å, α = 90.000, β = 108.579(3), γ = 90.000°, V = 3358.9(3) Å^3, Z = 2, T = 100.01 K, ρ_{calc} = 1.470 g cm^{-3}, μ = 2.042 mm^{-1}. Of a total of 5570 reflections that were collected, 5570 were unique. Final R_1 = 0.0452 and wR_2 = 0.1093. CCDC Number: 913422.

Crystal Parameters for $Ex^2Box{\subset}(Anthracene)_{0.5}{\cdot}4PF_6$(anthracene). $[C_{60}H_{48}N_4{\subset}(C_{14}H_{10})_{0.5}{\cdot}(PF_6)_4]{\cdot}(C_{14}H_{10}){\cdot}(MeCN)_2$. Yellow block (0.25 × 0.10 × 0.05 mm). Triclinic, $P\bar{1}$, a = 10.061(3), b = 11.220(4), c = 21.754(7) Å, α = 77.931(18), β = 85.603(18), γ = 65.560(16)°, V = 2186.1(13) Å^3, Z = 1, T = 100.03 K, ρ_{calc} = 1.333 g cm^{-3}, μ = 0.184 mm^{-1}. Of a total of 59 360 reflections that were collected, 12 946 were unique. Final R_1 = 0.0898 and wR_2 = 0.2662. CCDC Number: 913425.

Crystal Parameters for $Ex^2Box{\subset}Pyrene{\cdot}4PF_6$(pyrene). $[C_{60}H_{48}N_4{\subset}C_{16}H_{10}{\cdot}(PF_6)_4]{\cdot}(C_{16}H_{10}){\cdot}(MeCN)_4$. Yellow block (0.22 × 0.13 × 0.09 mm). Triclinic, $P\bar{1}$, a = 10.280(3), b = 11.369(3), c = 21.540(6) Å, α = 78.670(13), β = 84.909(13), γ = 64.499(13)°, V = 2227.88(11) Å^3, Z = 1, T = 100.03 K, ρ_{calc} = 1.471 g cm^{-3}, μ = 0.190 mm^{-1}. Of a total of 61 143 reflections that were collected, 12 838 were unique. Final R_1 = 0.0910 and wR_2 = 0.2082. CCDC Number: 913426.

Crystal Parameters for $Ex^2Box{\subset}(Tetraphene)_{0.5}{\cdot}4PF_6$(tetraphene)$_{0.5}$. $[C_{60}H_{48}N_4{\subset}(C_{18}H_{12})_{0.5}{\cdot}(PF_6)_4]{\cdot}(C_{18}H_{12})_{0.5}{\cdot}(MeCN)_3$. Colorless block (0.11 × 0.08 × 0.04 mm). Triclinic, $P\bar{1}$, a = 10.415(7), b = 11.339(9), c = 21.467(14) Å, α = 79.584(18), β = 85.427(13), γ = 65.790(2)°, V = 2274.0(3) Å^3, Z = 1, T = 99.98 K, ρ_{calc}

dx.doi.org/10.1021/ja4052763 | J. Am. Chem. Soc. 2013, 135, 12736–12746

Scheme 1. Two-Step Synthesis of $Ex^2Box{\cdot}4PF_6$ Starting from Extended 4,4′-Bipyridine Ex^2BIPY[a]

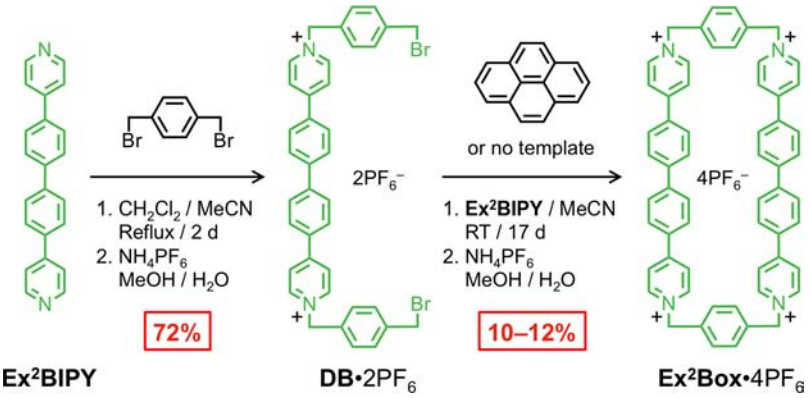

[a]Both the nontemplated and pyrene (6 equiv)-templated reaction of intermediate **DB**·$4PF_6$ (1 equiv) with Ex^2BIPY (1 equiv) in the second step afforded the desired $Ex^2Box{\cdot}4PF_6$ in similar 10−12% yields.

= 1.283 g cm^{-3}, μ = 1.595 mm^{-1}. Of a total of 14 610 reflections that were collected, 7508 were unique. Final R_1 = 0.1060 and wR_2 = 0.3191. CCDC Number: 936766.

Crystal Parameters for $Ex^2Box\subset Chrysene{\cdot}4PF_6$(chrysene). $[C_{60}H_{48}N_4\subset C_{18}H_{12}{\cdot}(PF_6)_4]{\cdot}(C_{18}H_{12}){\cdot}(MeCN)_4$. Colorless block (0.19 × 0.10 × 0.01 mm). Triclinic, $P\bar{1}$, a = 10.480(4), b = 11.349(5), c = 21.442(9) Å, α = 80.25(3), β = 86.77(3), γ = 64.519(2)°, V = 2268.6(17) $Å^3$, Z = 1, T = 100.12 K, ρ_{calc} = 1.483 g cm^{-3}, μ = 1.687 mm^{-1}. Of a total of 14 871 reflections that were collected, 7507 were unique. Final R_1 = 0.0447 and wR_2 = 0.1137. CCDC Number: 936767.

Crystal Parameters for $Ex^2Box\subset Tetracene{\cdot}4PF_6$(tetracene). $[C_{60}H_{48}N_4\subset(C_{18}H_{12}){\cdot}(PF_6)_4]{\cdot}(C_{18}H_{12}){\cdot}(MeCN)_4$. Orange block (0.23 × 0.10 × 0.02 mm). Triclinic, $P\bar{1}$, a = 10.480(3), b = 11.384(3), c = 21.556(6) Å, α = 80.426(2), β = 86.407(17), γ = 63.302(16)°, V = 2265.29(11) $Å^3$, Z = 1, T = 99.95 K, ρ_{calc} = 1.448 g cm^{-3}, μ = 1.689 mm^{-1}. Of a total of 14 958 reflections that were collected, 7309 were unique. Final R_1 = 0.0546 and wR_2 = 0.1575. CCDC Number: 913427.

Crystal Parameters for $Ex^2Box\subset(2,6\text{-Dinitrotoluene}){\cdot}4PF_6$. $[C_{60}H_{48}N_4\subset C_7H_6N_2O_4{\cdot}(PF_6)_4]$. Colorless block (0.17 × 0.08 × 0.03 mm). Orthorhombic, *Cmca*, a = 14.443(6), b = 38.482(14), c = 12.120(4) Å, α = 90.000, β = 90.000, γ = 90.000°, V = 6735.9(4) $Å^3$, Z = 4, T = 99.99 K, ρ_{calc} = 1.565 g cm^{-3}, μ = 2.125 mm^{-1}. Of a total of 13 160 reflections that were collected, 2799 were unique. Final R_1 = 0.0791 and wR_2 = 0.2195. CCDC Number: 913429.

Crystal Parameters for $Ex^2Box\subset(1,5\text{-Dinitronaphthalene}){\cdot}4PF_6$. $[C_{60}H_{48}N_4\subset C_{10}H_6N_2O_4{\cdot}(PF_6)_4]$. Yellow block (0.19 × 0.16 × 0.01 mm). Orthorhombic, *Cmca*, a = 14.913(6), b = 38.067(17), c = 12.106(5) Å, α = 90.000, β = 90.000, γ = 90.000°, V = 6872.8(5) $Å^3$, Z = 4, T = 100.01 K, ρ_{calc} = 1.569 g cm^{-3}, μ = 2.098 mm^{-1}. Of a total of 13 018 reflections that were collected, 3017 were unique. Final R_1 = 0.0422 and wR_2 = 0.0994. CCDC Number: 936768.

Crystal Parameters for $Ex^2Box\subset(9,10\text{-Anthraquinone})_{0.5}{\cdot}4PF_6$. $[C_{60}H_{48}N_4\subset(C_{14}H_{10}O_2)_{0.5}{\cdot}(PF_6)_4]{\cdot}MeCN$. Yellow block (0.05 × 0.05 × 0.03 mm). Monoclinic, $P2_1/c$, a = 20.082(37), b = 12.103(4), c = 14.458(6) Å, α = 90.000, β = 106.223(3), γ = 90.000°, V = 3374.2(2) $Å^3$, Z = 2, T = 100.01 K, ρ_{calc} = 1.528 g cm^{-3}, μ = 2.068 mm^{-1}. Of a total of 4115 reflections that were collected, 4115 were unique. Final R_1 = 0.0636 and wR_2 = 0.1751. CCDC Number: 913430.

Crystal Parameters for $Ex^2Box\subset(1,4\text{-Anthraquinone}){\cdot}4PF_6$. $[C_{60}H_{48}N_4\subset C_{14}H_8O_2{\cdot}(PF_6)_4]{\cdot}(CHCl_3)_2$. Yellow block (0.45 × 0.14 × 0.12 mm). Monoclinic, $P2_1/c$, a = 9.790(4), b = 14.131(6), c = 27.617(12) Å, α = 90.000, β = 95.911(2), γ = 90.000°, V = 3800.4(3) $Å^3$, Z = 2, T = 100.0 K, ρ_{calc} = 1.618 g cm^{-3}, μ = 0.421 mm^{-1}. Of a total of 57 735 reflections that were collected, 11 430 were unique. Final R_1 = 0.0722 and wR_2 = 0.2057. CCDC Number: 936769.

Crystal Parameters for $Ex^2Box\subset[1,4\text{-Bis}(3\text{-methoxyphenyl})\text{-}1H\text{-}1,2,3\text{-triazole}]{\cdot}4PF_6$[1,4-Bis(3-methoxyphenyl)-1*H*-1,2,3-triazole]. $[C_{60}H_{48}N_4\subset C_{16}H_{15}N_3O_2{\cdot}(PF_6)_4]{\cdot}(C_{16}H_{15}N_3O_2){\cdot}(MeCN)_{2.5}$. Colorless block (0.11 × 0.08 × 0.04 mm). Triclinic, $P\bar{1}$, a = 10.4059(3), b = 11.3697(3), c = 21.2021(5) Å, α = 81.1853(12), β = 86.2716(13), γ = 64.9951(11)°, V = 2246.50(10) $Å^3$, Z = 1, T = 100.03 K, ρ_{calc} = 1.530 g cm^{-3}, μ = 0.197 mm^{-1}. Of a total of 90 082 reflections that were collected, 13 104 were unique. Final R_1 = 0.1051 and wR_2 = 0.2775. CCDC Number: 936770.

Crystal Parameters for $Ex^2Box\subset(1,2,4\text{-Trichlorobenzene})_2{\cdot}4PF_6$(tetracene). $[C_{60}H_{48}N_4\subset(C_6H_3Cl_3)_2{\cdot}(PF_6)_4]{\cdot}(C_{18}H_{12}){\cdot}(MeCN)_4$. Yellow block (0.21 × 0.12 × 0.04 mm). Triclinic, $P\bar{1}$, a = 10.779(3), b = 11.107(3), c = 21.133(5) Å, α = 81.978(10), β = 88.551(10), γ = 67.138(10)°, V = 2307.3(10) $Å^3$, Z = 1, T = 99.99 K, ρ_{calc} = 1.555 g cm^{-3}, μ = 3.257 mm^{-1}. Of a total of 22 031 reflections that were collected, 7769 were unique. Final R_1 = 0.0435 and wR_2 = 0.1208. CCDC Number: 913423.

Crystal Parameters for $Ex^2Box\subset(1,5\text{-Dinaphtho}[38]\text{crown-}10){\cdot}4PF_6$. $[C_{60}H_{48}N_4\subset C_{36}H_{44}O_{10}{\cdot}(PF_6)_4]{\cdot}(MeCN)_8$. Orange block (0.47 × 0.13 × 0.08 mm). Triclinic, $P\bar{1}$, a = 10.821(3), b = 13.528(3), c = 21.903(6) Å, α = 88.571(13), β = 86.429(12), γ = 72.761(11)°, V = 3056.3(14) $Å^3$, Z = 1, T = 99.98 K, ρ_{calc} = 1.286 g cm^{-3}, μ = 1.398 mm^{-1}. Of a total of 24 907 reflections that were collected, 10 092 were unique. Final R_1 = 0.0562 and wR_2 = 0.1607. CCDC Number: 913424.

RESULTS AND DISCUSSION

The chemical constitution of Ex^2Box^{4+} (Figure 1a) is based on the family of 1,4-phenylene-bridged 4,4′-bipyridiniums,[14] referred to here as Ex^nBIPY^{2+} (n is the number of bridging phenylene rings). In the case of Ex^2Box^{4+}, two pyridinium rings are bridged by two (n = 2) phenylene rings—essentially a biphenylene subunit—to form Ex^2BIPY^{2+}, while two of these subunits are bridged by two *para*-xylylene moieties to form a tetracationic cyclophane which has a rectangular or box-like geometry. From its solid-state structure (Figure 1a), its width of 6.8 Å, or 3.4 Å when considering the van der Waals radius, is well suited[13,15] to the accommodation of π-conjugated aromatic guests, while its length of 18.9 Å allows a guest to be as long as 15.5 Å in relation to the van der Waals radii. In addition to this vast cavity of almost 2 nm in length, the backbone of Ex^2Box^{4+} is electronically nonuniform (Figure 1b), thus making it possible to match the electronic constitutions of guests with those of the receptor and exploit multiple modes of binding with the aim of increasing the affinity of Ex^2Box^{4+} toward a particular guest. The electrostatic potential map (Figure 1b) and the HOMO/LUMO electron density distribution (Figure 1c) of Ex^2Box^{4+}, obtained from density functional theory (DFT) calculations, show that the biphenylene subunit in the middle is more electronegative (the electron-rich region), while

dx.doi.org/10.1021/ja4052763 | J. Am. Chem. Soc. 2013, 135, 12736−12746

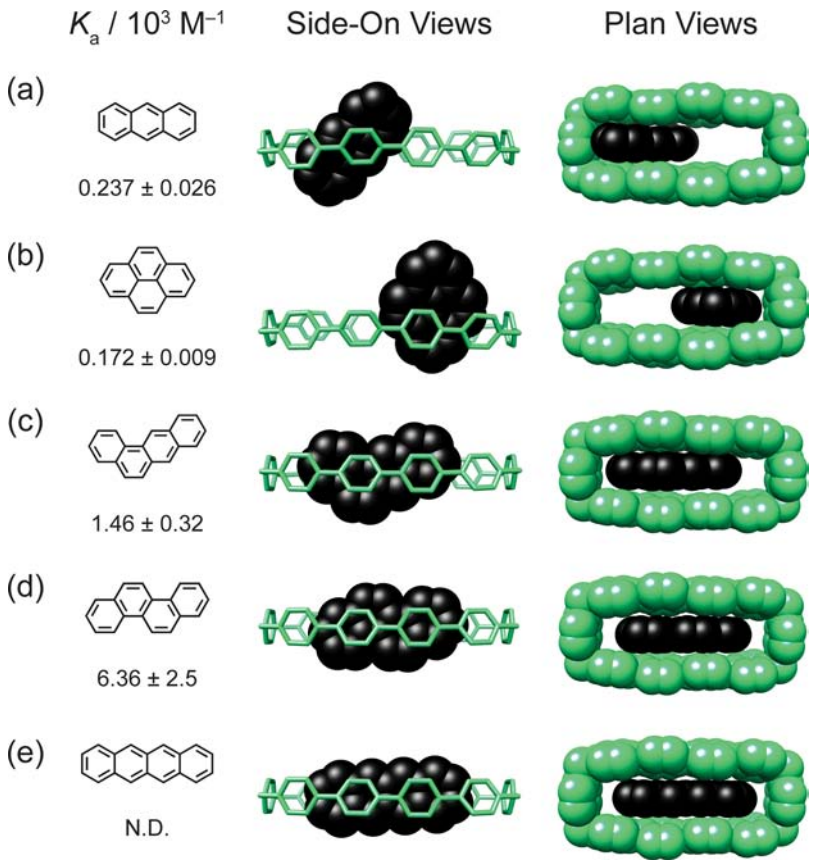

Figure 2. Structural formulas of the guests and the corresponding K_a values for binding inside Ex^2Box^{4+} obtained by ^1H NMR spectroscopy in CD_3CN (left) and the side-on (middle) and plan (right) views of the stick/space-filling representations of the solid-state superstructures of the complexes of Ex^2Box^{4+} with (a) anthracene, (b) pyrene, (c) tetraphene, (d) chrysene, and (e) tetracene. The hydrogen atoms, counterions, and solvent molecules are omitted for the sake of clarity. Color code: green = all atoms of Ex^2Box^{4+}; and black = the carbon atoms of the aromatic core of the guest. N.D. = not determined.

the pyridinium rings of Ex^2Box^{4+} are more electropositive (the electron-deficient region).

Synthesis and Complex Formation. $Ex^2Box{\cdot}4PF_6$ was synthesized (Scheme 1) using a modified procedure (see the Experimental Section) based on the preparation[15] of its shorter analogue, $ExBox{\cdot}4PF_6$. The synthesis was carried out by treating the extended bipyridine (**Ex²BIPY**) with an excess of α,α'-dibromo-*p*-xylene affording, after counterion exchange, the hexafluorophosphate salt $DB{\cdot}2PF_6$. Subsequently, the cyclization step was performed by using **Ex²BIPY** and $DB{\cdot}2PF_6$ (in a 1:1 ratio) following two synthetic pathways: pyrene-templated and nontemplated. Both methods led to the formation of the desired product $Ex^2Box{\cdot}4PF_6$ in comparable, 10−12%, yields. It should be noted that these yields are lower than those obtained[15] for $ExBox{\cdot}4PF_6$, 19 and 42% yields for the nontemplated and pyrene-templated procedures, respectively. This result indicates that no templation of Ex^2Box^{4+} occurs using pyrene as the template, and the 10−12% yield merely reflects the nontemplated pathway followed during the cyclization step. The decrease in yield (from 19% to 10−12%) for the nontemplated pathway when comparing $ExBox^{4+}$ with Ex^2Box^{4+} is most likely the result of the limited solubility of **Ex²BIPY** in the reaction medium (MeCN). Full characterization—NMR spectroscopy, HRMS, and XRD—of $Ex^2Box{\cdot}4PF_6$ was carried out (see the Experimental Section for a full synthetic description and characterization data for all the precursors).

In order to probe the concerted modes of binding in Ex^2Box^{4+}, various electron-rich polycyclic aromatic hydrocarbon (PAH) guests were first investigated, and their complexes with Ex^2Box^{4+} were studied in the solid state (XRD), in solution (^1H NMR/CD_3CN), and *in silico*. Single crystals of the 1:1 complexes of five guests—anthracene, pyrene, tetraphene, chrysene, and tetracene—with Ex^2Box^{4+} were obtained by slow vapor diffusion of iPr_2O into the solution of the corresponding "1:1 complex" in MeCN, and the XRD analysis (see Figure 2) of these crystals reveals the binding diversity exhibited by Ex^2Box^{4+}.

Considering all five PAH guests investigated, each demonstrates a different behavior in the solid state from that observed[15] in the case of $ExBox^{4+}$. Instead of being aligned along one side of the cyclophane, which would lead to charge-transfer and van der Waals interactions, anthracene and pyrene are positioned (Figure 2a,b, respectively) at angles of ∼45° and 90°, respectively, protruding from the cavity of Ex^2Box^{4+}. By comparison,[15] both anthracene and pyrene are almost fully aligned along its long axis inside the cavity of $ExBox^{4+}$. By contrast, tetraphene, chrysene, and tetracene, which can overlap with all four pyridinium rings of Ex^2Box^{4+} and assist in charge-transfer interactions on each end, are aligned (Figure 2c−e, respectively) inside Ex^2Box^{4+} but not inside $ExBox^{4+}$ since the length (11.3 Å, van der Waals) of the latter is not sufficient to accommodate guests longer than anthracene (11.3 Å, van der Waals). Out of the three, chrysene and tetracene are centered

dx.doi.org/10.1021/ja4052763 | J. Am. Chem. Soc. 2013, 135, 12736−12746

Table 1. Binding Parameters of the Ex^2Box^{4+}⊂Guest Complexes

	binding parameters		
guest	$K_a/10^3$ (M^{-1})[a]	E (kcal mol^{-1})[d]	ΔE_{rel} (kcal mol^{-1})[e]
anthracene	0.237 ± 0.026	−20.7	−9.9
pyrene	0.172 ± 0.009	–	–
tetraphene	1.46 ± 0.32	–	–
chrysene	6.36 ± 2.5	–	–
tetracene	–[b]	−25.8	−14.7
DNT	0.022 ± 0.010	–	–
DNN	0.042 ± 0.021	–	–
9,10-AQ	0.463 ± 0.018	−21.4	−10.3
1,4-AQ	0.825 ± 0.106	−23.7	−12.6
BMPT	0.836 ± 0.013	–	–
TCB	–[c]	–	–
DN38C10	1.11 ± 0.063	–	–

[a]Determined by ^{1}H NMR spectroscopy (CD_3CN; $CDCl_3$ for the guests with limited solubility in CD_3CN; all at 298 K). [b]Binding affinity could not be determined on account of solubility restrictions. [c]Binding affinity was too low for detection. [d]Energy determined by DFT calculations. [e]Relative energy compared to the complex of Ex^2Box^{4+} with four MeCN molecules (E = −11.1 kcal mol^{-1}) determined by DFT calculations.

inside Ex^2Box^{4+}, while tetraphene is positioned closer to one end of the cavity.

Binding studies in solution support the observations in the solid state. By comparing the values of the binding affinities (Table 1) for the five studied PAHs, obtained by ^{1}H NMR titration in CD_3CN, anthracene and pyrene have significantly lower K_a values (237 and 172 M^{-1}, respectively) than those (1.46×10^3 and 6.36×10^3 M^{-1}, respectively) observed for tetraphene and chrysene; the K_a value for tetracene could not be determined because of solubility restrictions. The K_a values for binding of anthracene and pyrene inside Ex^2Box^{4+} are also lower than those (883 and 7.16×10^3 M^{-1}, respectively) obtained with $ExBox^{4+}$ and explain why no templation was observed (Scheme 1) during the synthesis of $Ex^2Box{\cdot}4PF_6$ by using pyrene. These observations are in agreement with the fact that only charge-transfer interactions on one end of the cavity occur when anthracene and pyrene bind inside Ex^2Box^{4+}. Moreover, the pyridinium rings in Ex^2Box^{4+} are separated by two relatively electron-rich phenylene rings, which decrease their electron deficiency, and thus their affinities toward electron-rich guests, when only one end of Ex^2Box^{4+} can assist in charge-transfer interactions. This hypothesis is further supported by the fact that relatively weak charge-transfer bands are observed (Figure S17) in the absorption spectra for the complexes of Ex^2Box^{4+} with anthracene and pyrene.

When comparing the binding affinities of tetraphene and chrysene inside $ExBox^{4+}$ and Ex^2Box^{4+}, the K_a values (1.46×10^3 and 6.36×10^3 M^{-1}, respectively) for Ex^2Box^{4+} are higher than those (914 and 2.32×10^3 M^{-1}, respectively) for $ExBox^{4+}$. This significant increase in binding affinity, by a factor of ∼2, can be attributed to the favorable alignment of the guests inside Ex^2Box^{4+}, which is not possible in the case of $ExBox^{4+}$, allowing for more effective charge-transfer interactions. The smaller K_a value (1.46×10^3 M^{-1}) for the binding of tetraphene inside Ex^2Box^{4+} when compared with that (6.36×10^3 M^{-1}) of chrysene is possibly a result of the noncentered position of tetraphene inside the cavity (Figure 2c) and/or different solvophobic effects. To find a possible explanation as to why anthracene and pyrene do not align inside Ex^2Box^{4+} in the solid state, a series of DFT calculations have been carried out using anthracene as the model system.

DFT Calculations. In order to understand the relative energetics which govern the mode of solid-state binding within the elongated Ex^2Box^{4+} cavity, the geometry of the Ex^2Box^{4+}⊂anthracene complex in Figure 2a was optimized in the Poisson−Boltzmann solvation model[16] for MeCN (ε = 37.5 and R_0 = 2.18 Å) at the level[17] of M06-2X/6-311G with Jaguar 7.5 to calculate the relative energies (E) associated with moving (Figure 3a) the anthracene guest over some distance (d) along the length of the Ex^2Box^{4+} cavity. After moving the guest, relative to the host, the position of the anthracene center was fixed, and both the host and guest were allowed to relax to find the lowest-energy co-conformation of the 1:1 complex. Starting from the crystal superstructure (Figure 3a; "crystal-like co-conformation"), it is possible to calculate the relative energies of the 1:1 complex as the anthracene guest is moved gradually toward the center position (0.0 Å) of the cyclophane. As this movement is enacted, a global energetic minimum, where the guest is ∼2.5 Å away from the 0.0 Å position of Ex^2Box^{4+}, is reached. This energy minimum occurs as a consequence of the ideal overlap between one of the terminal benzenoid rings of anthracene with the pyridinium rings of the host in addition to the slipped $\pi-\pi$ stacking interactions that occur between the biphenylene bridges in the host with the remaining two benzenoid rings of anthracene. Once the moving guest molecule reaches the 0.0 Å position of the cyclophane, the potential energy reaches a global maximum, indicating that the donor−acceptor interactions near the pyridinium rings of the cyclophane contribute the most in relation to the overall binding of the 1:1 complex. If the anthracene guest is moved beyond the 0.0 Å position to the other end of the cyclophane, then the relative energy levels mirror, as expected, that of the opposite end. Essentially, the co-conformation observed in the solid state corresponds to the local minimum when the semiorthogonal anthracene guest is allowed to overlap with the π-electron-poor pyridinium rings of Ex^2Box^{4+}. This co-conformation is 1.25 kcal mol^{-1} higher in energy than that of the global minimum when the guest is mostly aligned with the viologen subunits of Ex^2Box^{4+}. Thus, any π-electron-rich guest that is incapable of overlapping with both of the π-electron-poor pockets can only enter into favorable charge-transfer interactions and polarization (interaction between a charge and an induced dipole) at one of the ends of the cyclophane.[18]

In order to determine whether or not an electron-poor guest can bind inside Ex^2Box^{4+}, a similar calculation (Figure 3b) for the 1:1 complex of Ex^2Box^{4+}⊂9,10-anthraquinone reveals an analogous mirror-like behavior between the relative energy levels when the guest is positioned at either end of the cyclophane. The difference in binding 9,10-anthraquinone (9,10-AQ), however, lies in the fact that the central quinone portion introduces a π-electron-poor region in the guest molecule that forces the global minimum to exist ∼2.5 Å away from the central 0.0 Å position (similar to anthracene) of Ex^2Box^{4+} and the next (local) minimum to exist ∼1.5 Å from the central position. This co-conformation is different from that observed computationally for anthracene and can be attributed to favorable van der Waals interactions—and not charge-transfer interactions—between Ex^2Box^{4+} and 9,10-AQ.

When the guest molecule is changed from 9,10-AQ to the constitutional isomer 1,4-AQ (Figure 3c)—the only guest with a net dipole moment (2.65 D as determined by gas-phase

dx.doi.org/10.1021/ja4052763 | J. Am. Chem. Soc. 2013, 135, 12736−12746

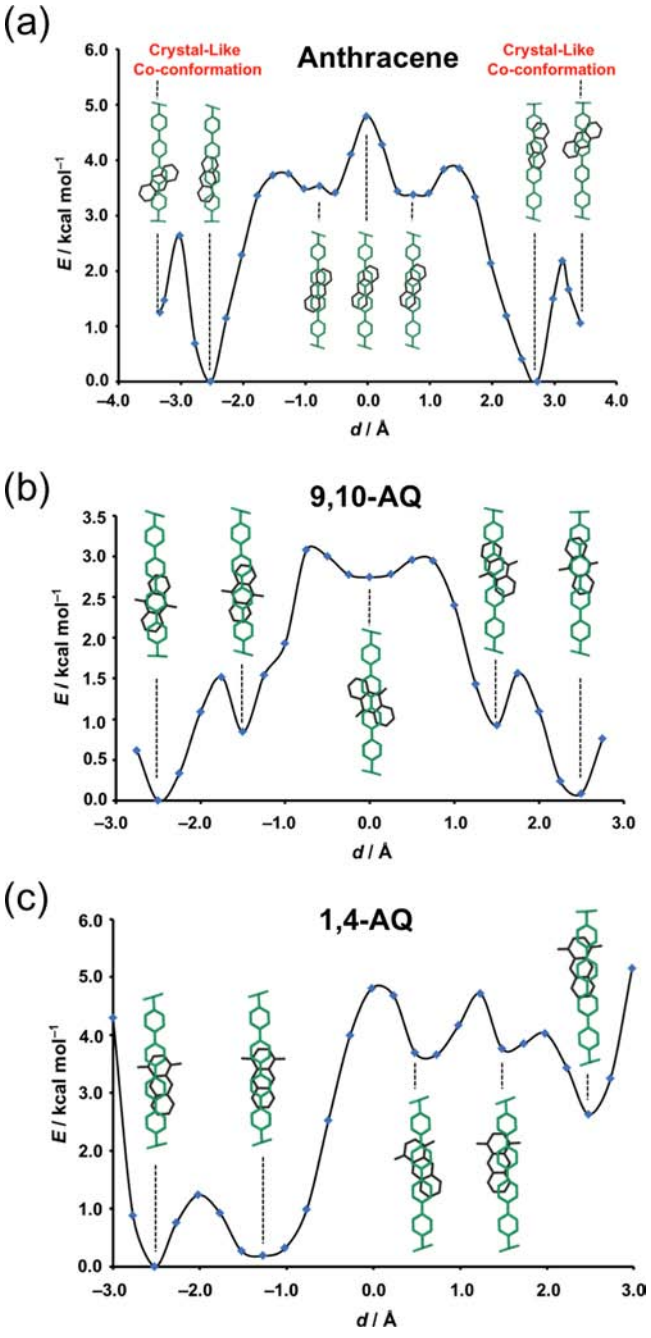

Figure 3. Optimized superstructures of the complexes (a) Ex^2Box^{4+}⊂anthracene, (b) Ex^2Box^{4+}⊂9,10-AQ, and (c) Ex^2Box^{4+}⊂1,4-AQ and the relative energies (E) associated with the different potential binding motifs were explored using DFT at the M06-2X/6-311G level. After moving the guest molecule some distance (d/Å) along the length of the viologen subunit of Ex^2Box^{4+}, the center position of the guest molecule was fixed relative to the center position of the cyclophane, and both the host and guest were allowed to relax to find the lowest-energy co-conformation of the 1:1 complex.

calculations)—the symmetry of the relative energy levels between the two halves of the cyclophane, not surprisingly, is lost. In this particular case, the global energy minimum occurs when the guest molecule capitalizes on the favorable dipole–quadrupole (electrostatic) interactions between the guest and the host, in addition to the interactions between the electron-poor quinone portion of the guest with the biphenylene subunits of the cyclophane, while the terminal aromatic ring of 1,4-AQ overlaps simultaneously with the pyridinium rings of Ex^2Box^{4+}. When the guest molecule is moved toward the center 0.0 Å position of the cyclophane, a global energy maximum is obtained where the overlapping of the host–guest orbitals is disfavored, presumably as a result of its losing the van der Waals interactions between the terminal aromatic ring of the guest with the pyridinium rings of the host and the dipole–quadrupole interaction of the complex. As 1,4-AQ is moved through the central cyclophane position, local minima are observed at ∼0.5, 1.5, and 2.5 Å; these co-conformations, however, remain significantly higher in energy relative to when the quinone portion of the guest overlaps with the biphenylene subunit of the cyclophane and the terminal aromatic ring of the guest overlaps with the pyridinium rings of the cyclophane.

Figure 4 illustrates the plan and side-on views of the frontier molecular orbitals of the 1:1 host–guest complexes of Ex^2Box^{4+}⊂anthracene (a), Ex^2Box^{4+}⊂tetracene (b), and Ex^2Box^{4+}⊂9,10-AQ (c). In the case of electron-rich anthracene and tetracene, the HOMO resides on the guest molecule, while the LUMO is located on the host, and the HOMO–LUMO energy difference ($\Delta E_{HOMO-LUMO}$) of the complexes is 4.43 and 3.90 eV, respectively. The $\Delta E_{HOMO-LUMO}$ for the anthracene complex is greater than that for the tetracene complex on account of anthracene possessing fewer π-electrons than tetracene, resulting in a lower HOMO energy level. When the guest is more electron-poor, as is the case with 9,10-AQ, then the HOMO resides on the biphenylene subunit of Ex^2Box^{4+} and the LUMO on 9,10-AQ, and the $\Delta E_{HOMO-LUMO}$ is 5.18 eV. This energy difference is larger than those for anthracene and tetracene, indicating that the affinity is not based primarily on charge-transfer interactions, an observation which is further supported by a complete lack of a charge-transfer band in the absorption spectrum (Figure S17) of Ex^2Box^{4+}⊂9,10-AQ. Thus, the binding affinity between Ex^2Box^{4+} and 9,10-AQ is attributed to the van der Waals interactions, namely, intermolecular polarization.

Analysis (Figure 5a,b) of the frontier molecular orbitals between Ex^2Box^{4+} and 1,4-AQ demonstrates a similar result to that observed in the case of 9,10-AQ, where the HOMO resides on Ex^2Box^{4+} and the LUMO is located on 9,10-AQ. The $\Delta E_{HOMO-LUMO}$ gap is 5.17 eV, resulting once again in the lack of a charge-transfer band in the absorption spectrum of the 1:1 complex. These data suggest that the binding observed between Ex^2Box^{4+} and 1,4-AQ also occurs on account of favorable electrostatic and other van der Waals interactions. Rotating (Figure 5c) 1,4-AQ inside the cavity of Ex^2Box^{4+} so that the quinone portion overlaps with the pyridinium rings of the cyclophane in preference to the biphenylene subunit results in the loss of the dipole–quadrupole interaction, which increases the energy of the complex by 3.8 kcal mol^{-1}.

These computational results suggest that the complexation of an electron-rich guest inside the cavity of Ex^2Box^{4+} favors a co-conformation which maximizes its orbital overlap with the pyridinium rings on account of favorable charge-transfer interactions, while the binding of an electron-poor guest prefers to adopt a co-conformation which maximizes favorable van der Waals interactions. A comparison of these different modes of binding was made by calculating the complexation energies (Table 1) for the four complexes to find that the strengths increase in the following order: anthracene (−9.9 kcal mol^{-1}), 9,10-AQ (−10.3 kcal mol^{-1}), 1,4-AQ (−12.6 kcal mol^{-1}), and tetracene (−14.7 kcal mol^{-1}). Although 9,10-AQ and 1,4-AQ capitalize on the electrostatic and other van der

dx.doi.org/10.1021/ja4052763 | J. Am. Chem. Soc. 2013, 135, 12736–12746

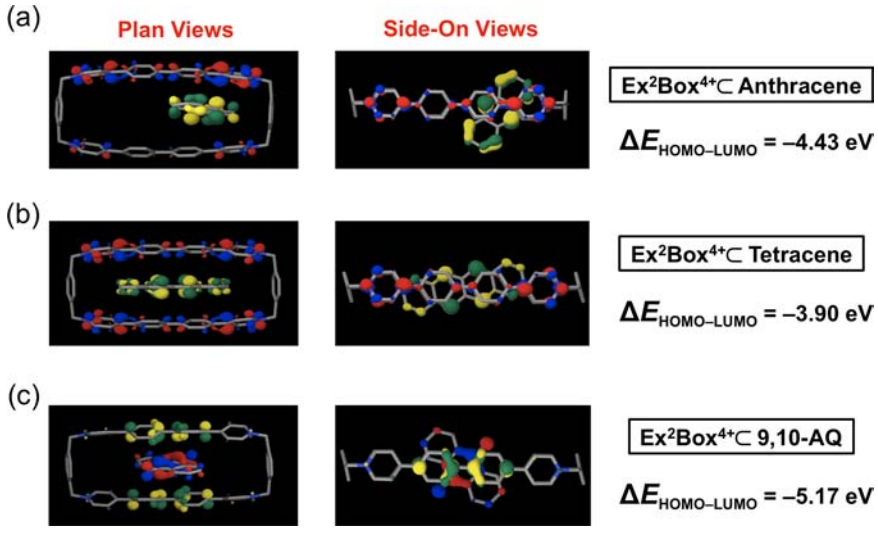

Figure 4. Plan and side-on views of the frontier molecular orbitals of the 1:1 host–guest complexes of (a) $\mathbf{Ex^2Box^{4+}}$⊂anthracene, (b) $\mathbf{Ex^2Box^{4+}}$⊂tetracene, and (c) $\mathbf{Ex^2Box^{4+}}$⊂9,10-AQ. In each case, the yellow and green colored orbitals represent the HOMO, and the red and blue colored orbitals represent the LUMO of the 1:1 complexes. The HOMO–LUMO energy difference ($\Delta E_{\mathrm{HOMO-LUMO}}$) of each complex is also provided (right).

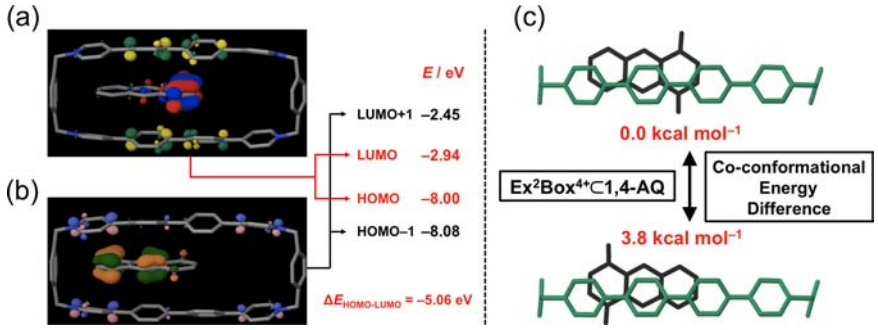

Figure 5. Plan views of the frontier molecular orbitals of the 1:1 complex of $\mathbf{Ex^2Box^{4+}}$⊂1,4-AQ (a,b). The yellow and green colored orbitals represent the HOMO, and the red and blue colored orbitals represent the LUMO of the 1:1 complex. The energy values (eV) for the first and second HOMO/LUMO levels are provided to the right of the orbital figures in (a) and (b). The relative energy difference associated with the rotation (c) of 1,4-AQ inside the cavity of $\mathbf{Ex^2Box^{4+}}$ is demonstrated; it is an action, which results in the overlap of the electron-poor quinone portion of the guest with one set of pyridinium rings of the cyclophane. This co-conformation is 3.8 kcal mol^{-1} higher relative to the initial position, which started with the quinone portion of the guest overlapping with the biphenylene subunit of the host.

Waals interactions, these calculations predict higher binding affinities for these guests compared to anthracene, an observation which demonstrates that the accumulation of multiple weak interactions can result in higher binding affinities over fewer and weakened charge-transfer interactions. The highest value, in the case of tetracene, is in agreement with its predicted high affinity for $\mathbf{Ex^2Box^{4+}}$ based on the smallest $\Delta E_{\mathrm{HOMO-LUMO}}$, since the molecule is long enough to reach both ends of the viologen subunits of the host.

In line with the results obtained from the DFT calculations (Figures 3–5), the importance of interactions other than charge-transfer becomes evident (Figure 6) experimentally when $\mathbf{Ex^2Box^{4+}}$ is cocrystallized with π-electron-poor guests, namely, 2,6-dinitrotoluene (DNT), 1,5-dinitronaphthalene (DNN), 9,10-AQ, and 1,4-AQ. Three out of four electron-deficient guests (specifically, DNT, DNN, and 9,10-AQ) crystallized as inclusion complexes wherein the guests reside (Figure 6a–c, respectively) in the middle of the $\mathbf{Ex^2Box^{4+}}$ cavity and overlap optimally with the relatively electron-rich biphenylene subunits of the cyclophane. In the case of 1,4-AQ, the guest is positioned (Figure 6d) at one end, or in the "pocket", of the $\mathbf{Ex^2Box^{4+}}$ cavity such that the naphthalene subunit maximizes its overlap with the pyridinium rings and the quinone subunit overlaps with the biphenylene bridge. The position and orientation of 1,4-AQ inside $\mathbf{Ex^2Box^{4+}}$ are in a close agreement (Figure 3c) with the DFT prediction. In the case of 9,10-AQ, the guest resides in the middle of the cyclophane, which is, according (Figure 3b) to the DFT results, one of the local energy minima. The global-minimum co-conformation for 9,10-AQ occurs when it is aligned at one end of the cyclophane in a similar fashion to both anthracene and 1,4-AQ.

Comparing Complex Stabilities. The relatively low K_a values (Figure 6a–d, Table 1) for electron-deficient guests support the theory that the charge-transfer interactions are not present when an electron-deficient guest binds inside $\mathbf{Ex^2Box^{4+}}$; this observation supports the results obtained from DFT calculations. The K_a values of the electron-deficient guests become larger as the size of the aromatic core increases, indicating the growing significance of the van der Waals interactions inside $\mathbf{Ex^2Box^{4+}}$ in the case of these guests. The smallest one-ring guest, DNT, has a K_a value of 22 M^{-1}, while

dx.doi.org/10.1021/ja4052763 | J. Am. Chem. Soc. 2013, 135, 12736–12746

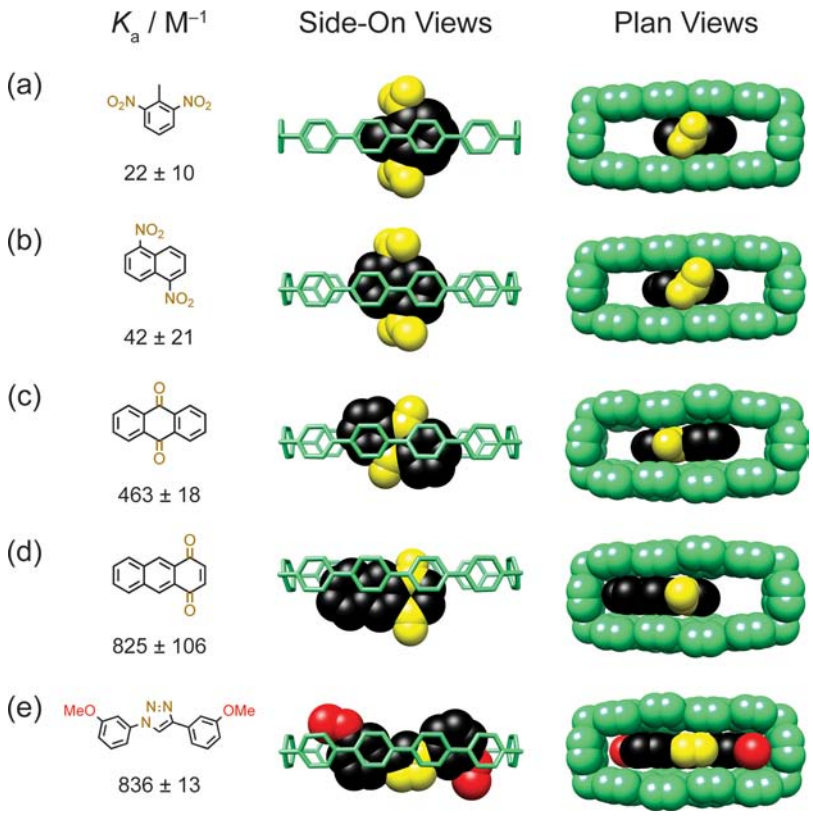

Figure 6. Structural formulas of the guests and the corresponding K_a values for binding inside $\mathbf{Ex^2Box^{4+}}$ obtained by ^{1}H NMR spectroscopy in CD_3CN (left) and the side-on (middle) and plan (right) views of the stick/space-filling representations of the solid-state superstructures of the complexes of $\mathbf{Ex^2Box^{4+}}$ with (a) DNT, (b) DNN, (c) 9,10-AQ, (d) 1,4-AQ, and (e) BMPT. The hydrogen atoms, counterions, and solvent molecules are omitted for the sake of clarity. Color code: green = all atoms of $\mathbf{Ex^2Box^{4+}}$; black = the carbon atoms of the aromatic core of the guest; yellow = electron-deficient substituents/subunits (NO_2, C═O, N−N═N); and red = electron-rich substituents (OMe).

9,10-AQ and 1,4-AQ have the K_a values of 463 and 825 M^{-1}, respectively. In summary, it can be concluded that various van der Waals interactions, such as ion−dipole, dipole−dipole, and/or favorable orbital overlaps,[19−21] are the main contributors to the binding affinities of these guests.

The results obtained (Figures 3 and 6, respectively) from the binding studies of both π-electron-rich and -poor guests inside $\mathbf{Ex^2Box^{4+}}$ indicate that a K_a value larger than 10^3 M^{-1} can be achieved with the assistance of either the charge-transfer interactions occurring simultaneously at each end of the cyclophane (tetraphene and chrysene) or favorable van der Waals interactions (1,4-AQ). In further support of this theory, 1,4-bis(3-methoxyphenyl)-1*H*-1,2,3-triazole (BMPT) was designed and synthesized, and its binding properties inside $\mathbf{Ex^2Box^{4+}}$ were investigated (Figure 6e) in the solid state and in solution. BMPT is nearly linear, possessing two electron-rich 3-methoxyphenyl rings on either side of the electron-deficient 1*H*-1,2,3-triazole (triazole) ring in the middle. The electronic structure of BMPT can, therefore, assist in charge-transfer interactions at each end of the cyclophane and favorable van der Waals interaction in the middle. As hypothesized, the K_a value of BMPT is almost 10^3 (836 M^{-1}), and the guest is fully aligned (Figure 6e) inside the cavity of $\mathbf{Ex^2Box^{4+}}$ in the solid state.

As both 9,10-AQ and BMPT show good solubility in MeCN and their K_a values were higher than that of pyrene, they were tested as templates in the last step of the synthesis of $\mathbf{Ex^2Box}\cdot 4PF_6$. The isolated yields for $\mathbf{Ex^2Box}\cdot 4PF_6$ when using 9,10-AQ and BMPT as the templates were 15% and 20%, respectively, showing an increase in yields in tune with the greater binding affinity (463 and 836 M^{-1}, respectively) of the template.

The alignment of the larger guests, such as, tetraphene, chrysene, and BMPT, inside $\mathbf{Ex^2Box^{4+}}$ is also observed in solution (CD_3CN) as indicated by ^{1}H NMR spectroscopy. The ^{1}H NMR spectra of the 1:1 complexes of $\mathbf{Ex^2Box^{4+}}$ with chrysene and BMPT are shown in Figure 7. Both complexes display upfield shifts for the signals corresponding to the β, γ, and δ protons of $\mathbf{Ex^2Box^{4+}}$ and all of the signals for the protons of the guests, in addition to a small downfield shift for the resonances associated with the *para*-xylylene (C_6H_4) protons of $\mathbf{Ex^2Box^{4+}}$. This effect is caused by π-electron shielding of the face-to-face oriented aromatic rings, which occurs upon complexation. The signals for the α and CH_2 protons of $\mathbf{Ex^2Box^{4+}}$ display very little or no movements in their ^{1}H NMR spectra since these protons are located in the pockets of $\mathbf{Ex^2Box^{4+}}$ and are therefore not affected significantly by the shielding effect of the aromatic guests. This behavior is in good agreement with the inclusion of the guests inside the cavity of $\mathbf{Ex^2Box^{4+}}$.

The difference in the chemical shifts for the individual proton signals (H_1−H_6) of bound and unbound chrysene was investigated, and the results are in agreement (Figure 7b) with the fully aligned orientation (Figure 2d) of the guest inside $\mathbf{Ex^2Box^{4+}}$. All six proton signals display upfield change in chemical shift because of the π-electron shielding of the face-to-face oriented aromatic rings. Protons H_2−H_4 are additionally shielded by the *para*-xylylene rings at each end of the cyclophane. Of the three protons H_2−H_4, proton H_3 should

dx.doi.org/10.1021/ja4052763 | J. Am. Chem. Soc. 2013, 135, 12736−12746

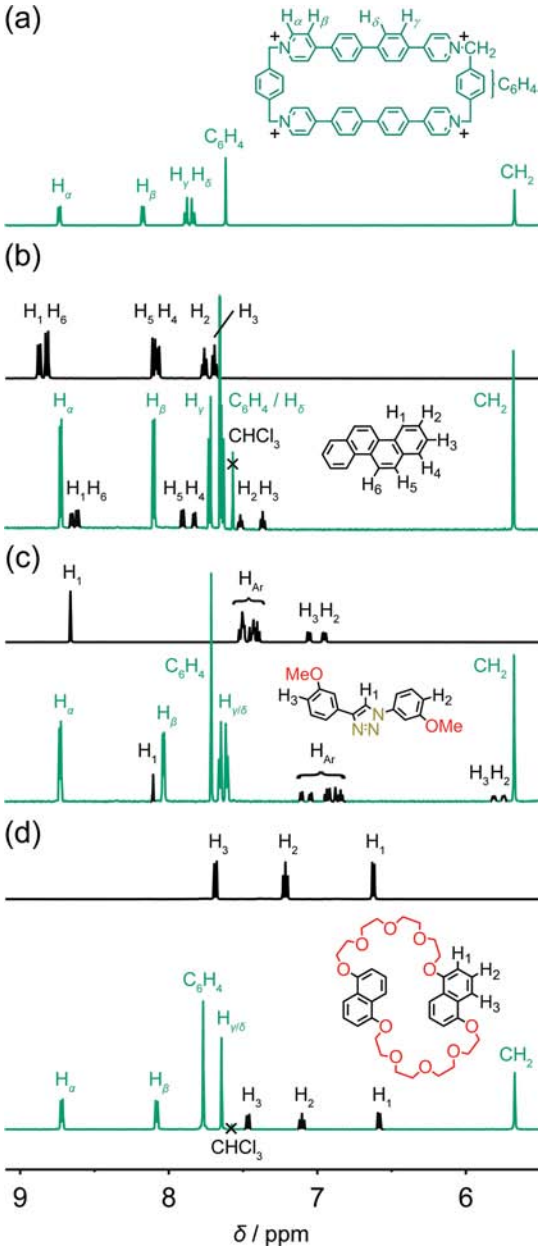

Figure 7. Partial ^{1}H NMR spectra of (a) **Ex^{2}Box^{4+}** and its 1:1 complexes with (b) chrysene, (c) BMPT, and (d) DN38C10 recorded in CD_3CN (containing ~10% of $CDCl_3$ (b,d) for the purposes of solubility) at 298 K on a 600 MHz spectrometer. The ^{1}H NMR spectrum (black) of the unbound guest in CD_3CN is shown above the ^{1}H NMR spectrum of the 1:1 complex (green for the **Ex^{2}Box^{4+}** and black for the bound-guest signals) in (b–d).

be shielded the most since it resides near the center of the *para*-xylylene ring. The observed differences in the chemical shifts for each proton follow exactly this predicted order: (i) 0.34 ppm for proton H_3, (ii) 0.25–2.26 ppm for protons H_2 and H_4, and (iii) 0.20–0.22 ppm for protons H_1, H_5, and H_6. Similar behavior was observed (Figure 7c) in the case of BMPT. According to the fully aligned orientation (Figure 6e) of the guest inside **Ex^{2}Box^{4+}**, protons H_2 and H_3 in BMPT should display the largest upfield shifts. Indeed, a difference in chemical shifts of 1.15 and 1.11 ppm was observed for protons H_2 and H_3, respectively, while all other protons displayed upfield change in chemical shift in the range of 0.38–0.52 ppm.

The ability of **Ex^{2}Box^{4+}** to accommodate (i) two guests or (ii) two subunits of a single macrocycle inside its cavity is illustrated in Figure 8. The solid-state superstructures of a one-ring guest, 1,2,4-trichlorobenzene (TCB, Figure 8a), and a two-ring guest, 1,5-dinaphtho[38]crown-10 (DN38C10, Figure 8b) were obtained from X-ray crystallographic analysis of the single crystals of the corresponding complexes. Single crystals of the complex of **Ex^{2}Box^{4+}** with two TCB molecules were obtained quite unintentionally while attempting to grow crystals of the complex of **Ex^{2}Box^{4+}** and tetracene, where TCB was present as the solvent! The solid-state superstructure (Figure 8a) shows that **Ex^{2}Box^{4+}**, in contrast to **ExBox^{4+}**, has enough space to encapsulate two guests; the two TCB molecules inside the cavity are in close contact yet are not held together by hydrogen bonds (Figure 8a, highlighted in blue). DN38C10 provides an example (Figure 8b) in which two dioxynaphthalene units within the same molecule allow for an even more effective binding inside **Ex^{2}Box^{4+}**. Each dioxynaphthalene unit is positioned as close as possible to the electron-deficient pyridinium rings on each side to allow for the maximum charge-transfer overlap, which is the predominant mode of binding in **Ex^{2}Box^{4+}**. The fact that the K_a value (1.11×10^3 M^{-1}) for DN38C10 is higher than those for anthracene and pyrene by an order of magnitude and is comparable to the values for anthracene and pyrene bound inside **ExBox^{4+}** demonstrates yet again that two charge-transfer interactions within a 1:1 complex are required to observe binding on the order of 10^3.

By comparing the extent (Figure 7d) of the shielding effect for protons H_1–H_3 of DN38C10, one can determine the preferred mode of binding in solution. For example, the signal for the H_3 protons of DN38C10 is shifted upfield by 0.22 ppm when comparing it with that for the unbound guest, while the resonance for the H_1 protons is shifted by only 0.03 ppm and the signal for the H_2 protons by 0.11 ppm. These observations imply the close-to-perpendicular orientation of the naphthalene units of DN38C10 inside **Ex^{2}Box^{4+}** (the shielding effect decreases as the distance between the proton and cavity increases) and are in agreement with the mode of binding observed (Figure 8b) in the solid state.

CONCLUSIONS

We have shown that **Ex^{2}Box^{4+}** is capable of binding both π-electron-rich (predominantly charge-transfer interactions) and -poor (predominantly van der Waals interactions) guests on account of their electronic interplay with the host's pyridinium moieties, separated by biphenylene subunits. Such versatility in a large synthetic host, combined with a simple design, has many potential advantages. Not only is it possible for **Ex^{2}Box^{4+}** to form ternary complexes with two small guests, as demonstrated in the case of 1,2,4-trichlorobenzene, but it is also possible to bind strongly large macrocyclic polyethers such as dinaphtho[38]crown-10 on account of the presence of two covalently linked π-electron-rich subunits in the form of dioxynaphthalene moieties. This recognition could be particularly useful in the realm of the template directed,[22] stepwise synthesis of topologically challenging molecular knots. Since the length of **Ex^{2}Box^{4+}** is almost 2 nm, it can potentially encapsulate graphene nanoribbons[23] that are as wide as four fused rings—the length of tetracene—for the purposes of nanoribbon exfoliation. Moreover, when converted to the water-soluble chloride salt, **Ex^{2}Box**·4Cl may be able to serve as a phase-transfer catalyst for both π-electron-rich and -poor

dx.doi.org/10.1021/ja4052763 | J. Am. Chem. Soc. 2013, 135, 12736–12746

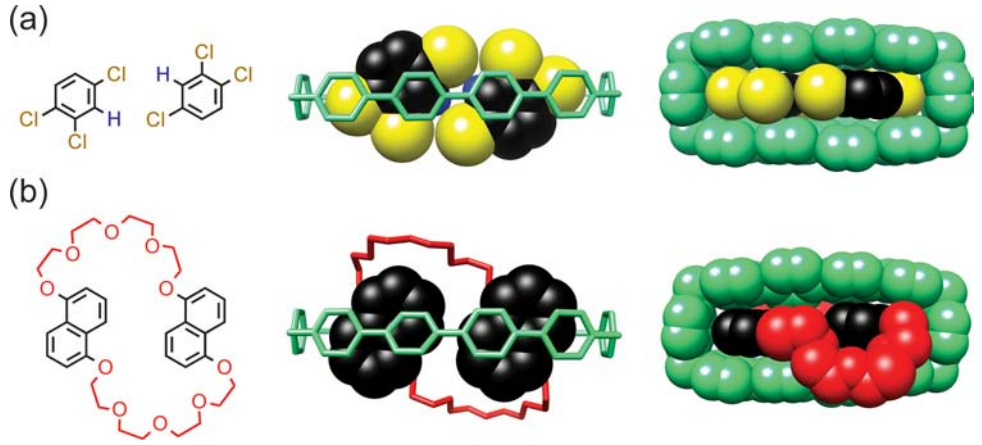

Figure 8. Structural formulas of the guests (left) and the side-on (middle) and plan (right) views of the stick/space-filling representations of the solid-state superstructures of the complexes of $\mathbf{Ex^2Box^{4+}}$ with (a) TCB and (b) DN38C10. The hydrogen atoms, counterions, and solvent molecules are omitted for the sake of clarity. Color code: green = all atoms of $\mathbf{Ex^2Box^{4+}}$; black = the carbon atoms of the aromatic core of the guest; yellow = the chlorine atom; and red = the polyether chain.

guests that are insoluble in aqueous environments. By taking advantage of the synergistic nature of $\mathbf{Ex^2Box^{4+}}$, guests of varying sizes and electronic compositions can be matched so as to exploit multifarious interactions. Gaining a more fundamental understanding of synergistic binding modes in synthetic receptors could make it possible one day to mimic the unrivaled affinity and specificity that is characteristic of the enzyme–substrate relationship.

■ ASSOCIATED CONTENT

Ⓢ Supporting Information

Detailed synthetic procedures and characterization (NMR and HRMS) data for all compounds, crystallographic and spectroscopic (NMR, CV, and UV–vis) characterization for $\mathbf{Ex^2Box}\cdot 4PF_6$ and the corresponding inclusion complexes. This material is available free of charge via the Internet at http://pubs.acs.org.

■ AUTHOR INFORMATION

Corresponding Author

wag@wag.caltech.edu; stoddart@northwestern.edu

Author Contributions

⊥M.J. and J.C.B. contributed equally.

Notes

The authors declare no competing financial interest.

■ ACKNOWLEDGMENTS

The data reported are tabulated in the Supporting Information and the crystallographic parameters of each single crystal were deposited into the Cambridge Crystallographic Data Centre (CCDC). The research at Northwestern University (NU) was enabled by the National Center for Nano Technology Research at the King Abdulaziz City for Science and Technology (KACST) in Saudi Arabia. The authors thank Dr. Turki S. Al-Saud and Dr. Nezar H. Khdary at KACST for their interest in this research. J.F.S. is supported by the Non-Equilibrium Energy Research Center (NERC), which is an Energy Frontier Research Center (EFRC) funded by the U.S. Department of Energy, Office of Basic Energy Sciences (DOE-BES) under award DESC0000989. M.J. gratefully acknowledges The Netherlands Organization for Scientific Research (NWO) and the Marie Curie Cofund Action (Rubicon Fellowship). J.C.B. is supported by a National Defense Science and Engineering Graduate Fellowship (32 CFR 168a) from the Department of Defense (DoD) and gratefully acknowledges receipt of a Ryan Fellowship from the NU International Institute for Nanotechnology (IIN). E.J.D., N.L.S., and C.J.B. are supported by a Graduate Research Fellowship (GRF) from the National Science Foundation (NSF).

■ REFERENCES

(1) (a) Pedersen, C. J. *J. Am. Chem. Soc.* **1967**, *89*, 2495–2496; 7017–7036. (b) Pedersen, C. J. *J. Am. Chem. Soc.* **1970**, *92*, 386–391. (c) Pedersen, C. J. *J. Am. Chem. Soc.* **1970**, *92*, 391–394. (d) Pedersen, C. J. *Angew. Chem., Int. Ed. Engl.* **1988**, *27*, 1021–1027.

(2) (a) Bright, D.; Truter, M. R. *Nature* **1970**, *225*, 176–177. (b) Bright, D.; Truter, M. R. *J. Chem. Soc. B* **1970**, 1544–1550. (c) Frensdorff, H. K. *J. Am. Chem. Soc.* **1970**, *93*, 600–606. (d) Bush, M. A.; Truter, M. R. *J. Chem. Soc. B* **1971**, 1440–1446. (e) Pedersen, C. J. *Aldrichimica Acta* **1971**, *4*, 1–4. (f) Pedersen, C. J.; Frensdorff, H. K. *Angew. Chem., Int. Ed. Engl.* **1972**, *11*, 16–25.

(3) Cram, D. J. *Angew. Chem., Int. Ed. Engl.* **1988**, *27*, 1009–1020.

(4) Lehn, J.-M. *Angew. Chem., Int. Ed. Engl.* **1988**, *27*, 89–112.

(5) (a) Cram, D. J.; Cram, J. M. *Science* **1974**, *183*, 803–809. (b) Cram, D. J. *Science* **1983**, *219*, 1177–1183. (c) Cram, D. J.; Cram, J. M. *Container Molecules and Their Guests*; Royal Society of Chemistry: Cambridge, U.K., 1994.

(6) (a) Lehn, J.-M. *Science* **1985**, *227*, 849–856. (b) Lehn, J.-M. *Angew. Chem., Int. Ed. Engl.* **1990**, *29*, 1304–1319. (c) Lehn, J.-M. *Supramolecular Chemistry Concepts and Perspectives*; Wiley-VCH: Weinheim, Germany, 1995; (d) Beer, P. D.; Gale, P. A.; Smith, D. K. *Supramolecular Chemistry*; Oxford University Press: Oxford, U.K., 1999; (e) Steed, J. W.; Atwood, J. L. *Supramolecular Chemistry*; Wiley-VCH: Weinheim, Germany, 2009; (f) Stoddart, J. F. *Nat. Chem.* **2009**, *1*, 14–15.

(7) (a) Alston, D. R.; Slawin, A. M. Z.; Stoddart, J. F.; Williams, D. J.; Zarzycki, R. *Angew. Chem., Int. Ed. Engl.* **1988**, *27*, 1184–1185. (b) Stoddart, J. F. *Carbohydr. Res.* **1989**, *192*, 12–15. (c) Harada, A.; Li, J.; Kamachi, M. *Nature* **1992**, *356*, 325–327. (d) Wenz, G. *Angew. Chem., Int. Ed. Engl.* **1994**, *33*, 803–822. (e) Szejtli, J. *Chem. Rev.* **1998**, *98*, 1743–1753. (f) Nepogodiev, S. A.; Stoddart, J. F. *Chem. Rev.* **1998**, *98*, 1959–1976. (g) Harada, A. *Acc. Chem. Res.* **2001**, *34*, 456–464. (h) Ravoo, B. J.; Jacquier, J.-C.; Wenz, G. *Angew. Chem., Int. Ed.* **2003**, *42*, 2066–2070. (i) Dodziuk, H. *Cyclodextrins and Their Complexes: Chemistry, Analytical Methods, Applications*; Wiley-VCH: Weinheim, Germany, 2006; (j) Harada, A.; Kobayashi, R.; Takashima, Y.; Hashidzume, A.; Yamaguchi, H. *Nat. Chem.* **2011**, *3*, 34–37.

(8) (a) Freeman, W. A.; Mock, W. L.; Shih, N.-Y. *J. Am. Chem. Soc.* **1981**, *103*, 7367−7368. (b) Mock, W. L.; Shih, N.-Y. *J. Am. Chem. Soc.* **1989**, *111*, 2697−2699. (c) Kim, J.; Jung, I.-S.; Kim, S.-Y.; Lee, E.; Kang, J.-K.; Sakamoto, S.; Yamaguchi, K.; Kim, K. *J. Am. Chem. Soc.* **2000**, *122*, 540−541. (d) Kim, K. *Chem. Soc. Rev.* **2002**, *31*, 96−107. (e) Lee, J. W.; Samal, S.; Selvapalam, N.; Kim, H.-J.; Kim, K. *Acc. Chem. Res.* **2003**, *36*, 621−630. (f) Lagona, J.; Mukhopadhyay, P.; Chakrabarti, S.; Isaacs, L. *Angew. Chem., Int. Ed.* **2005**, *44*, 4844−4870. (g) Liu, S.; Zavalij, P. Y.; Isaacs, L. *J. Am. Chem. Soc.* **2005**, *127*, 16798−16799. (h) Kim, K.; Selvapalam, N.; Ko, Y.-H.; Park, K.-M.; Kim, D.; Kim, J. *Chem. Soc. Rev.* **2007**, *36*, 267−279. (i) Issacs, L. *Chem. Commun.* **2009**, 619−629. (j) Gao, C.; Silvi, S.; Ma, X.; Tian, H.; Credi, A.; Venturi, M. *Chem.—Eur. J.* **2012**, *18*, 16911−16921. (k) Lee, T.-C.; Kalenius, E.; Lazar, A. I.; Assaf, K. I.; Kuhnert, N.; Grün, C. H.; Jänis, J.; Scherman, O. A.; Nau, W. M. *Nat. Chem.* **2013**, *5*, 376−382.

(9) (a) Gutsche, C. D.; Dhawan, B.; No, K. H.; Muthukrishnan, R. *J. Am. Chem. Soc.* **1981**, *103*, 3782−3792. (b) Gutsche, C. D. *Acc. Chem. Res.* **1983**, *16*, 161−170. (c) Shinkai, S. *Tetrahedron* **1993**, *49*, 8933−8908. (d) Ikeda, A.; Shinkai, S. *Chem. Rev.* **1997**, *97*, 1713−1734. (e) Bew, S. P.; Burrows, A. D.; Düren, T.; Mahon, M. F.; Moghadam, P. Z.; Sebestyen, V. M.; Thurston, S. *Chem. Commun.* **2012**, *48*, 4824−4826.

(10) (a) Ogoshi, T.; Kanai, S.; Fujinami, S.; Yamagishi, T.-A.; Nakamoto, Y. *J. Am. Chem. Soc.* **2008**, *130*, 5022−5023. (b) Cao, D.; Kou, Y.; Liang, J.; Chen, Z.; Wang, L.; Meier, H. *Angew. Chem., Int. Ed.* **2009**, *48*, 9721−9724. (c) Strutt, N. L.; Forgan, R. S.; Spruell, J. M.; Botros, Y. Y.; Stoddart, J. F. *J. Am. Chem. Soc.* **2011**, *133*, 5668−5671. (d) Cragg, P. J.; Sharma, K. *Chem. Soc. Rev.* **2012**, *41*, 597−607. (e) Strutt, N. L.; Fairen-Jimenez, D.; Iehl, J.; Lalonde, M. B.; Snurr, R. Q.; Farha, O. K.; Hupp, J. T.; Stoddart, J. F. *J. Am. Chem. Soc.* **2012**, *134*, 17436−17439.

(11) (a) *The Porphyrin Handbook*; Kadish, K. M.; Smith, K. M.; Guilard, R.; Eds.; Academic: San Diego, 2003; (b) Sessler, J. L.; Seidel, D. *Angew. Chem., Int. Ed.* **2003**, *42*, 5134−5175. (c) Saito, S.; Osuka, A. *Angew. Chem., Int. Ed.* **2011**, *50*, 4342−4373. (d) O'Sullivan, M. C.; Sprafke, J. K.; Kondratuk, D. V.; Rinfray, C.; Claridge, T. D. W.; Saywell, A.; Blunt, M. O.; O'Shea, J. N.; Beton, P. H.; Malfois, M.; Anderson, H. L. *Nature* **2011**, *469*, 72−75.

(12) (a) Diederich, F.; Dick, K. *Angew. Chem., Int. Ed. Engl.* **1983**, *22*, 715−716. (b) Diederich, F.; Dick, K. *Angew. Chem., Int. Ed. Engl.* **1984**, *23*, 810−812. (c) Diederich, F.; Dick, K. *J. Am. Chem. Soc.* **1984**, *106*, 8024−8036. (d) Bühner, M.; Geuder, W.; Gries, W.-K.; Hünig, S.; Koch, M.; Poll, T. *Angew. Chem., Int. Ed. Engl.* **1988**, *27*, 1553−1556. (e) Diederich, F. *Cyclophanes*; The Royal Society of Chemistry: Cambridge, 1991.

(13) (a) Odell, B.; Reddington, M. V.; Slawin, A. M. Z.; Spencer, N.; Stoddart, J. F.; Williams, D. J. *Angew. Chem., Int. Ed. Engl.* **1988**, *27*, 1547−1550. (b) Asakawa, M.; Dehaen, W.; Labbé, G.; Menzer, S.; Nouwen, J.; Raymo, F. M.; Stoddart, J. F.; Williams, D. J. *J. Org. Chem.* **1996**, *61*, 9591−9595. (c) Sue, C.-H.; Basu, S.; Fahrenbach, A. C.; Shveyd, A. K.; Dey, S. K.; Botros, Y. Y.; Stoddart, J. F. *Chem. Sci.* **2010**, *1*, 119−125. (d) Barnes, J. C.; Fahrenbach, A. C.; Dyar, S. M.; Frasconi, M.; Giesener, M. A.; Zhu, Z.; Liu, Z.; Hartlieb, K. J.; Carmieli, R.; Wasielewski, M. R.; Stoddart, J. F. *Proc. Natl. Acad. Sci. U.S.A.* **2012**, *109*, 11446−11551.

(14) (a) Takahashi, K.; Nihira, T.; Akiyama, K.; Ikegami, Y.; Fukuyo, E. *J. Chem. Soc., Chem. Commun.* **1992**, 620−622. (b) Porter, W. W.; Vaid, T. P.; Rheingold, A. L. *J. Am. Chem. Soc.* **2005**, *127*, 16559−16566. (c) Kolivoška, V.; Gál, M.; Pospíšil, L.; Valášek, M.; Hromadová, M. *Phys. Chem. Chem. Phys.* **2011**, *13*, 11422−11429.

(15) Barnes, J. C.; Juríček, M.; Strutt, N. L.; Frasconi, M.; Sampath, S.; Giesener, M. A.; McGrier, P. L.; Bruns, C. J.; Stern, C. L.; Sarjeant, A. A.; Stoddart, J. F. *J. Am. Chem. Soc.* **2013**, *135*, 183−192.

(16) Tannor, D. J.; Marten, B.; Murphy, R.; Friesner, R. A.; Sitkoff, D.; Nicholls, A.; Ringnalda, M.; Goddard, W. A., III; Honig, B. *J. Am. Chem. Soc.* **1994**, *116*, 11875−11882.

(17) *Jaguar*; Schrödinger, LLC, New York, NY, 2007.

(18) This kind of binding motif was also observed experimentally in the crystal superstructure (Figure 2b) of the 1:1 complex between Ex^2Box^{4+} and pyrene.

(19) Toyota, S.; Woods, C. R.; Benaglia, M.; Haldimann, R.; Wärnmark, K.; Hardcastle, K.; Siegel, J. S. *Angew. Chem., Int. Ed.* **2001**, *40*, 751−754.

(20) Martinez, C. R.; Iverson, B. L. *Chem. Sci.* **2012**, *3*, 2191−2201.

(21) Hunter, C. A.; Sanders, J. K. M. *J. Am. Chem. Soc.* **1990**, *112*, 5525−5534.

(22) Forgan, R. S.; Wang, C.; Friedman, D. C.; Spruell, J. M.; Stern, C. L.; Sarjeant, A. A.; Cao, D.; Stoddart, J. F. *Chem.—Eur. J.* **2012**, *18*, 202−212.

(23) Jiao, L.; Zhang, L.; Wang, X.; Diankov, G.; Dai, H. *Nature* **2009**, *458*, 877−880.